Journal of Computational Applied Mechanics 2024, 55 (1): 39-50

DOI: 10.22059/JCAMECH.2023.365756.883

RESEARCH PAPER

Performance Study of Partially Heated Annulus Filled with Two-Phase Nanofluid: Energy Perspective

Rouzbeh Mahmousi [a] , H. Pourmohamadian[b], M. Omidi Bidgoli[c, d, *]

[a] *Department of Mechanical Engineering, Yasouj University, Yasouj, Iran.*
[b] *Department of Mechanical Engineering, Naragh Branch, Islamic Azad University, Naragh, Iran.*
[c] *Department of Mechanical Engineering, University of Eyvanekey, Eyvanekey, Semnan, Iran.*
[d] *Department of Mechanical Engineering, Islamic Azad University, Badroud branch, Badroud, Isfahan, Iran.*

Abstract

In recent years, electrical appliances have become an integral part of human life, and efforts have been made to improve the quality and durability of electrical boards. One of the ways to improve the life of electrical boards is using cooling methods suitable for transferring the heat generated by the boards. In this paper, three different models of Case 1, Case 2, and Case 3 have been analyzed to provide an optimal model with the highest average Nusselt number. To achieve the optimal model the effect of heat source, the characteristics of hot and cold barriers and their locations on the flow field, heat transfer between two horizontal concentric cylinders with the presence of nanofluids were investigated. The results have shown that for all volume fractions, the Nusselt number increases with rising Riley number, as well as for the inner and outer cylinder, the value of the average Nusselt number increases at a constant Riley number with rising the volume fraction from 0 to 0.8%. Therefore, the highest Nusselt number occurs in volume fraction of 0.8% and Riley number of 10^5.

Keywords: Energy analysis, Partial heating, Annulus, Elliptic cylinders, Two-Phase, Nanofluid.

1. INTRODUCTION

Fluid like water or oil including solid nanoparticles is known as the nanofluid, which these particles can be metals, oxides, carbides, carbon nanotubes, etc [1, 2]. It has been proved that the proper knowledge about the nanofluid behavior is crucial to assess their efficiency for heat transfer applications, which has caused researchers to pursue finding features of nanofluids under different conditions [3, 4]. Annular spaces are a suitable method of heat transfer that has been found in different sectors such as geothermal, solar, and nuclear energy. This appropriate performance has gotten the attention to draw for evaluating the impact of other factors such as the presence of nanofluids in heat transfer at these spaces [5]. In 2016, Tayebi and Chamkhahave used Cu-Al_2O_3/water hybrid nanofluids for fulling two confocal elliptic cylinders to study their influences on heat transfer. their numerical study has shown that Cu-Al_2O_3 /water hybrid nanofluids have better performance than Al_2O_3/water nanofluid in these spaces [6]. In another study, the impact of CuO– water nanofluid magnetohydrodynamic natural convection was simulated and analyzed by CVFEM, which the nanofluids properties were reached with the KKL model. As a result of using CuO – water in the presence of a magnetic field with increasing Rayleigh number a significant improvement in temperature gradient has been observed [7]. Angle orientation and eccentricity are two factors affecting the rate of heat transfer in annular spaces. Research shows that increasing buoyancy forces helps improve heat transfer. In addition, the nanoparticle effect boosts with increasing Lorentz forces [8]. In general, research on annular spaces focuses on providing a model with the ideal geometry and type of nanofluids. As another example, in numerical simulations on the heat transfer of the elliptic annuluses, three nanofluids including Al_2O_3, CuO, SiO_2 and ZnO has been investigated under different geometric conditions. Dawood et al. have reported that SiO was the most proper nanofluid in terms of heat transfer

* Correpondng Auhor's Email: mostafaomidibidgoli@gmail.com

under the diameter of particles of 20 nm and percentage of concentration of 4%. The point to consider in this study is related to the impact of geometry (concentration percentage) on choosing the suitable nanofluid type that should be considered in the design of cooling systems under nanofluids [9].

As mentioned, the effects of geometric shape on heat transfer are important, and it has caused research on fluid behavior around various objects with different materials and geometry to continue. Delhani et al. has investigated the heat transfer around a square barrier for different angles, which the results have illustrated that the higher the barrier angle, the higher the heat transfer rate [10]. Dhimana et al. have considered two types of boundary conditions, constant temperature, and constant flux, for a square barrier [11]. Farooji et al. have declared that the heat transfer rate decreased with increasing nanoparticle diameter. Another useful application of barriers is associated with hydromagnetic currents, which reduces the effect of the magnetic field damping the perturbations [12]. Wang and Chen numerically studied the heat transfer in a wavy-wall channel and found that for Reynolds less than 180 currents remain constant and for Reynolds larger than that due to the transition to turbulent current, a significant increase in heat transfer is observed [13]. Yin et al. numerically investigated the thermal-hydraulics parameters of air in corrugated channels to shift different phases between the upper and lower walls. The results showed that, as the shift of phases increases, the coefficient of friction and the Nusselt number decrease [14]. In other studies, Zhang and Che have simulated eight different turbulence models for evaluating the heat transfer in cross-corrugated plates, as well as the coefficient of friction, the Colburn coefficient, and the local Nusselt number have also analyzed [15].

In this numerical study, convective heat transfer between two elliptical cylinders filled with the AlOOH nanofluid for three different models was investigated. These three models, Case 1, Case 2, and Case 3 have diverse boundary conditions (internal cylindrical surface temperatures), which can be compared and found the most proper model.

2. NUMERICAL MODEL

In Figure 1, the space between walls of the elliptical cylinders filled with a nanofluid including water and AlOOH nanoparticles, which are in the thermal equilibrium state, is illustrated. The no-slip boundary conditions are considered on the cylinder walls. Moreover, the temperature of the outer cylinder wall is constant T_c^*, while the temperature of the inner cylinder wall varies according to the type of model under study, as shown in Figure 2. The arrangement of temperatures on inner surfaces is presented in Table 1.

Table 1. Temperatures of inner surfaces

	Left	Right	top	Bottom
Case 1	T_c^*	T_c^*	T_h^*	T_h^*
Case 2	T_h^*	T_h^*	T_c^*	T_c^*
Case 3	Diagonally			

The governing equations on the system including two-phase nanofluid flow and heat transfer in the annulus were considered as follows [16]:

$$\nabla\cdot(\rho_{nf}\cdot V_m)=0 \tag{1}$$

where ρnf is the nanofluid density and V_m is the mean velocity.

$$\nabla\cdot(\rho_{nf}\cdot V_m\cdot V_m)=-\nabla P+\nabla\cdot(\mu_{nf}\cdot\nabla V_m)+(M\cdot\nabla)\cdot B \tag{2}$$

where μ_{nf} is the nanofluid viscosity.

$$\nabla\cdot(\rho_{nf}\cdot cV_m\cdot T)=\nabla\cdot(k_{nf}\cdot\nabla T)+\mu_0(M\cdot\nabla)\cdot H \tag{3}$$

where ρ is the fluid density and V_m is the velocity and μ is the fluid viscosity.

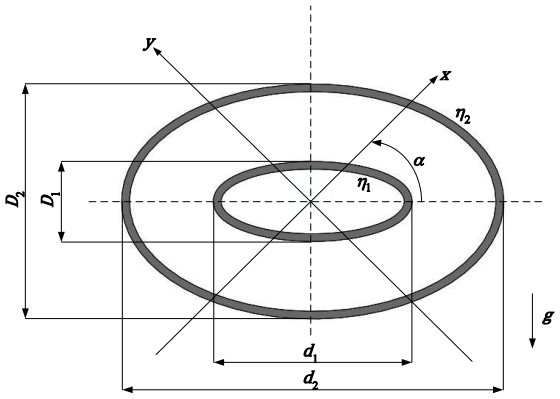

Figure 1. Problem schematic diagram

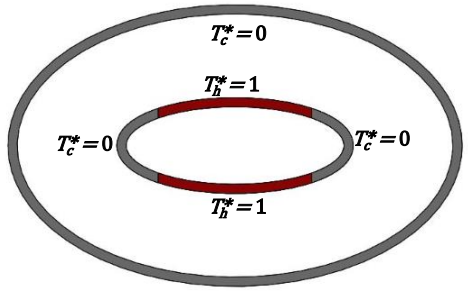

Case 1

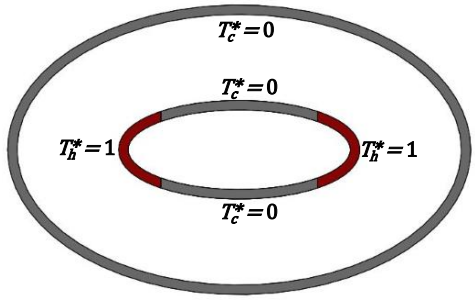

Case 2

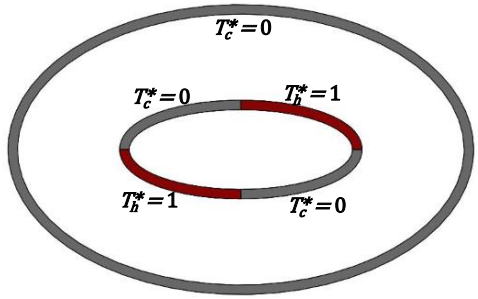

Case 3

Figure 2. Boundary conditions for the different studied cases.

The speculation of the dynamic viscosity behavior of the flow in the numerical solution field is analyzed using the power-law method in which the viscosity is defined as [16]:

$$\tau = K\dot{\gamma}^n \tag{4}$$

Constant thermophysical properties and incompressible conditions were presumed for the used nanofluid [17]:

Effective density

$$\rho_{nf} = (1-\phi)\rho_{bf} + \phi\rho_{np} \tag{5}$$

Heat capacity

$$(\rho \cdot c_p)_{nf} = (1-\phi)(\rho \cdot c_p)_{bf} + \phi(\rho \cdot c_p)_{np} \quad (6)$$

Thermal diffusivity

$$\alpha_{nf} = \frac{k_{nf}}{(\rho \cdot c_p)_{nf}} \quad (7)$$

Thermal expansion coefficient

$$(\rho \cdot \beta)_{nf} = (1-\phi)(\rho \cdot \beta)_{bf} + \phi(\rho \cdot \beta)_{np} \quad (8)$$

Thermal conductivity [18]:

$$\frac{k_{nf}}{k_f} = 1 + 4.4\mathrm{Re}_{np}^{0.4}\mathrm{Pr}^{0.66}\left(\frac{T}{Tfr}\right)^{10}\left(\frac{k_{np}}{k_{bf}}\right)^{0.03}\phi^{0.66} \quad (9)$$

Where φ is the volume fraction for the suspended nanoparticles, T_{fr} and T are the freezing point and the nanofluid temperature, Pr and R_{enp} are the Prandtl number in base fluid and the Reynolds number of the nanoparticle, respectively.

The Reynolds number of nanoparticles can be calculated more accurately by Equation (10):

$$\mathrm{Re}_{np} = \frac{\rho_{bf} \cdot u_B \cdot d_{np}}{\mu_{bf}} \quad (10)$$

Where d_{np} and μ_f are the nanoparticles diameter and the dynamic viscosity for the base fluid, u_B and ρ_f are the mean Brownian velocity of nanoparticle and density, respectively.

Provided that there is the absence of agglomeration, the nanoparticle Brownian velocity can be calculated with the following equation, which τ_d is the time required to cover the distance [18]:

$$\tau_d = \frac{d_{np}^2}{6D_B} \quad (11)$$

where D_B is the Brownian diffusion coefficient is given by bellow equation [18]:

$$D_B = \frac{k_b \cdot T}{3\pi \cdot \mu_{bf} \cdot d_{np}} \quad (12)$$

wherein $k_b = 1.38066 * 10^{-23}$ J/K is the Boltzmann constant.

$$u_B = \frac{2k_b \cdot T}{\pi \cdot \mu_{bf}^2 \cdot d_{np}} \quad (13)$$

by replacing Eq. (13) in Eq. (10), we obtain:

$$\mathrm{Re}_{np} = \frac{2\rho_{bf} \cdot k_b \cdot T}{\pi \cdot \mu_{bf}^2 \cdot d_{np}} \quad (14)$$

Dynamic viscosity [18]:

$$\frac{\mu_{nf}}{\mu_{bf}} = \left(1 - 34.87\left(\frac{d_{np}}{d_{bf}}\right)^{-0.3}\phi^{1.03}\right)^{-1} \quad (15)$$

$$d_{nf} = 0.1\left(\frac{6M}{N\pi\rho f_0}\right)^{-1} \quad (16)$$

$$M = \rho f_0 \forall m N \quad (17)$$

Where d_{nf} is the equivalent diameter of the fluid molecules under the normal temperature (T_0=293K) and ∀m ($(4/3)\pi[(df/2)]^3$), M and N are the molecular volume of fluid, molar mass, and the Avogadro number (N=6.022× 10^{-23} mol^{-1}), respectively [18].

In the present study, the finite volume method is utilized. In the numerical simulation, coupled equations of velocity-pressure are implemented. To reach a suitable accuracy in the numerical solution, second-order discretization,

as well as SIMPLEC algorithm, is taken into consideration. In all cases for all Reynolds number and volume frictions, to occupy less memory space on the computer and to economize the numerical solution process, the maximum 10^{-8} the remainder is used. The governing equations of the system were solved based on Eulerian-Eulerian single fluid Two-Phase Model (TPM) and with these assumptions that the coupling between phases is acceptable and particles closely follow the suspension flow. The two phases (fluid and solid) have been determined to be inter-penetrating and it means that each phase has its velocity field, and within any control volume there is a volume concentration of primary phase (fluid) and another volume concentration for the secondary phase (solid).

The elliptic shape is introduced with the metric coefficients including F, G, and H:

$$H = a\sqrt{sh^2(\eta)\sin^2(\theta)}$$
$$F = \frac{sh(\eta)\cos(\theta)}{\sqrt{sh^2(\eta)\sin^2(\theta)}} \quad (18)$$
$$G = \frac{ch(\eta)\sin(\theta)}{\sqrt{sh^2(\eta)\sin^2(\theta)}}$$

And the dimensionless variables:

$$H^* = \frac{H}{a},\ V_\eta^* = \frac{a}{\alpha f}V\eta,\ V_\theta^* = \frac{a}{\alpha f}V\theta$$
$$\psi^* = \frac{\psi}{\alpha f},\ \omega^* = \frac{a^2}{\alpha f},\ T^* = \frac{T - T_C}{T_h - T_C} \quad (19)$$

where a is the half elliptical focal distance:

$$a = \frac{d_1}{ch(\eta_1)} = \frac{d_2}{ch(\eta_2)} \quad (20)$$

In Table 2, the thermophysical properties used in this study are presented. In addition, Kuehn and Goldstein's empirical results were employed to validate the natural convection reached in this study [19] for $Ra_L = 2.09 \times 10^5$, Pr=5.45, ΔT=0.371 K, T_{ave}=303.18 K, and L/2ri=0.8 providing $T_i > T_o$. The comparisons for six temperature profiles at six different angles, (angle measured from the lower symmetry plane), are indicated in Figure 3.

Table 2. Thermophysical properties [19]

Material	ρ kg/m^3	c_p J/kg·K	k W/m·K	μ N·s/m^2
H_2O	998.2	4182.0	0.6	0.001003
AlOOH	3050.0	618.3	30.0	-

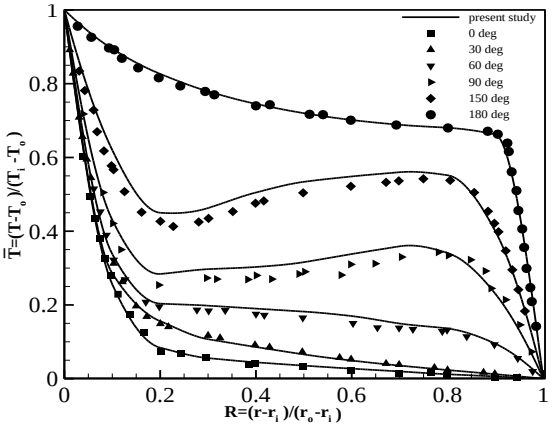

Figure 3. Variation of dimensionless temperature versus dimensionless radial distance: comparison between present work (solid lines) and experimental results of Kuehn and Goldstein [19] (symbols) that annulus is filled with water at steady-state conditions

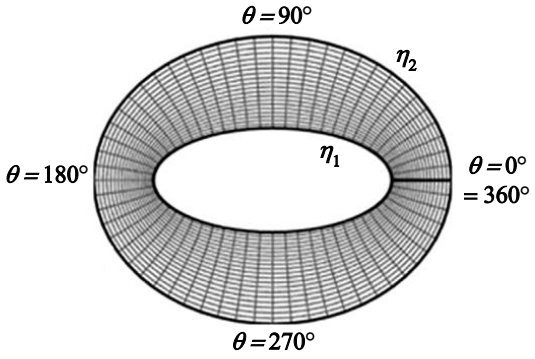

(a)

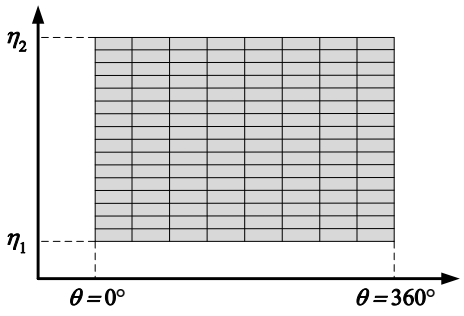

(b)

Figure 4. (a) Physical domain and (b) Computational domain

Table 3. Effect of number of nodes on Nu_{tot} for case 2D filled with water

Number of nodes	Ra=10^3	Ra=10^4	Ra=10^5
1,311	0.6412	1.1770	2.0017
2,606	0.6363	1.1601	1.9221
4,353	0.6347	1.1544	1.8896
6,575	0.6341	1.1525	1.8785
9,201	0.6337	1.1514	1.8720
10,319	0.6335	1.1508	1.8695
12,618	0.6335	1.1508	1.8695

3. RESULTS AND DISCUSSION

The heat transfer was evaluated for 3 2D models under different temperature conditions and in the presence of AlOOH–water nanofluid for volume fraction $0 < \phi < 0.08$ and Rayleigh number of $10^3 < Ra < 10^5$. The eccentricity of inner and outer ellipses are ε1=0.9 and ε2=0.6, respectively. As well, the Prandtl number and the orientation angle are Pr=6.2 and α=0° in turn. the finite-volume method (FVM) was utilized to gain local Nusselt numbers graphs, streamlines, and isotherms contours.

The streamlines and isotherms of Case 1, which have equal top and bottom surface temperatures for the inner ellipse, are demonstrated for different values of volume fractions and rayleigh numbers in Figure 5. The isotherms and streamlines graphs are shown the symmetric distributions for various volume fractions and Rayleigh numbers. Due to the dominant conduction mode in low Rayleigh numbers, drop-shaped temperature distributions have occurred near the heaters and generally, the impact of volume fractions for diverse values was low, whereas the higher the nanoparticle volume fraction, the higher the maximum values of stream function. In contrast, it can be seen that in Ra = 10^4, the plume shapes due to the dominant convection mode are formed near the heated ellipse surface. Increasing the volume fraction and Rayleigh have again caused the maximum stream function to rise and the plume became stronger. Also increasing the Rayleigh number got the symmetrical distribution to distort.

Figure 6 demonstrates the changes of the average Nusselt number with different Rayleigh numbers for the inner and outer cylinder of model 1. It is obvious that increasing rayleigh number and nanoparticle volume fraction lead to higher heat transfer. The average Nusselt number values less than 1 (Nuavg<1) on the inner and outer cylinder are due to the dominant conduction mode in the low Rayleigh number and the imposed cold temperature, respectively.

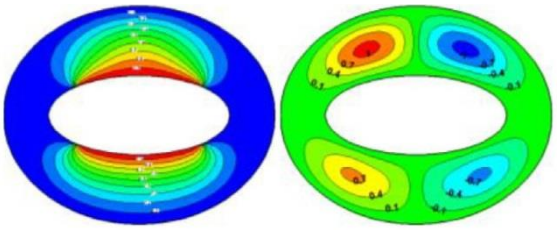

Ra=10^3 and ϕ=0

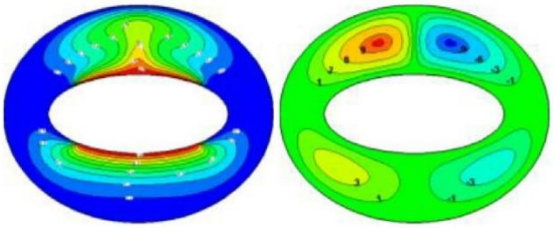

Ra=10^4 and ϕ=0.04

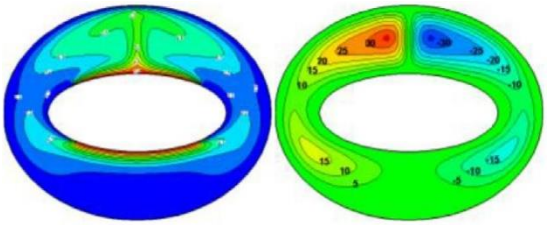

Ra=10^5 and ϕ=0.08

Figure 5. Isotherms (left) and streamlines (right) for different values of Rayleigh number Ra and volume fractions ϕ for Case 1

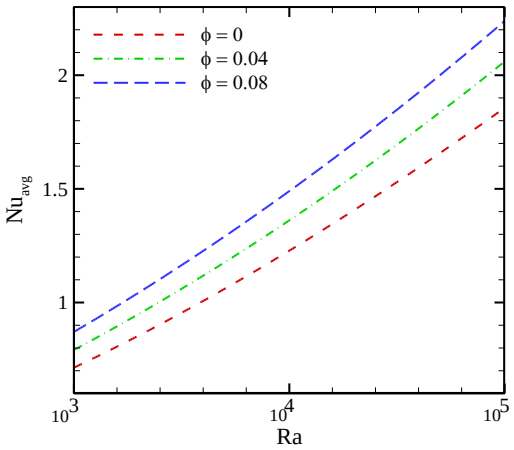

(a)

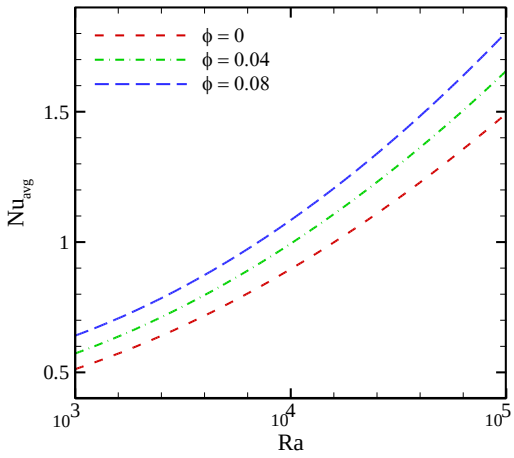

(b)

Figure 6. Effect of Rayleigh number Ra on average Nusselt number for different volume fractions ϕ (a) on the inner cylinder; (b) on the outer cylinder for Case 1

the streamlines and isotherms of Case 2, which have the equal left and right surface temperatures for the inner ellipse, are demonstrated for different values of volume fractions and rayleigh numbers in Figure 7. Rising the volume fraction and Rayleigh number increases the stream function values and does not distort the symmetric distribution even in the high Rayleigh number. It should be noted that employing nanofluids with high nanoparticles volume fractions is more effective.

Figure 8 demonstrates the changes of the average Nusselt number with different Rayleigh numbers for the inner and outer cylinder of model 2. It is evident that increasing rayleigh number and nanoparticle volume fraction lead to higher Nusselt number and heat transfer.

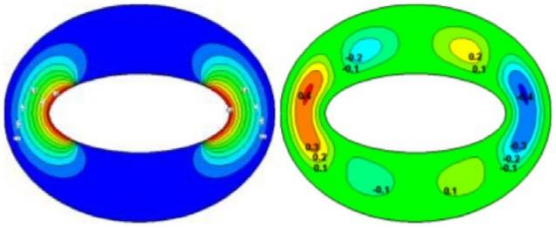

Ra=10^3 and ϕ=0

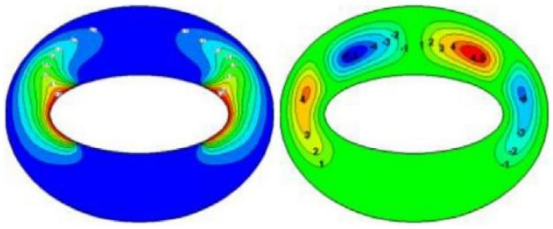

Ra=10^4 and ϕ=0.04

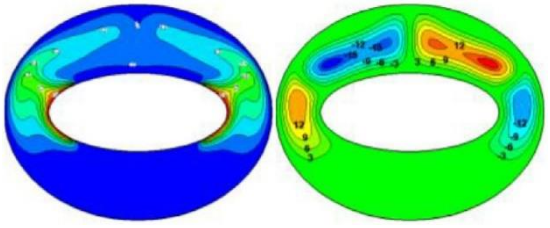

Ra=10^5 and ϕ=0.08

Figure 7. Isotherms (left) and streamlines (right) for different values of Rayleigh number Ra and volume fractions ϕ for Case 2

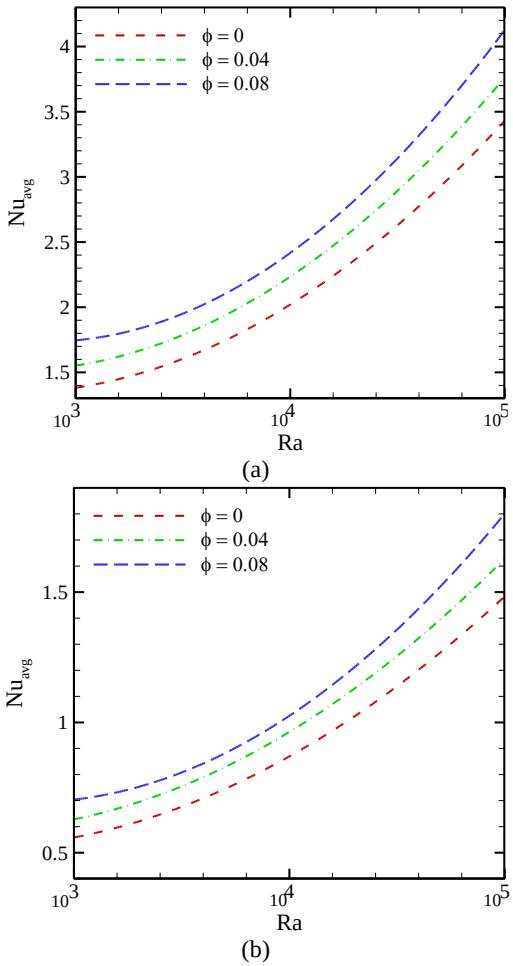

Figure 8. Effect of Rayleigh number Ra on average Nusselt number for different volume fractions ϕ (a) on the inner cylinder; (b) on the outer cylinder for Case 2

The isotherms and streamlines of Case 3, which have equal temperatures diagonally on the surface of the inner ellipse, are demonstrated for different values of volume fractions and rayleigh numbers in Figure 9. In this model, no symmetric state is seen for any parameter, and plume shapes become stronger by increasing the Rayleigh number due to the formation of drastic vortexes in the top right surface of the inner ellipse. Although stream function values increase with rising volume concentration, it does not affect streamlines and isotherms. The drop-shaped temperature distribution is formed above the heater due to the domination of the conduction mode of heat transfer at low Rayleigh numbers. Insignificant changes are formed by variations of nanoparticle volume fraction.

However, boosting nanoparticle volume concentration causes the maximum values of stream function to increase. On the contrary, the plume-like temperature distribution is formed above the top side of the inner ellipse at $Ra=10^4$ due to the convection mode of heat transfer. However, the temperature distribution is almost ellipsoidal under the inner ellipse due to gravity. Similar behavior is seen between nanoparticle volume concentration and Rayleigh numbers with the maximum values of stream function in terms of the increase or decrease. Symmetrical distribution is not observed by raising the numbers of Rayleigh.

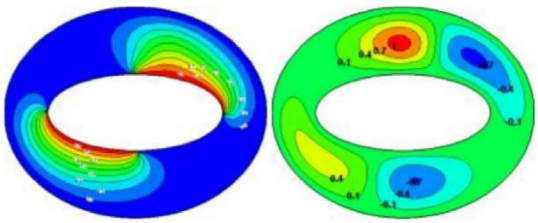

$Ra=10^3$ and $\phi=0$

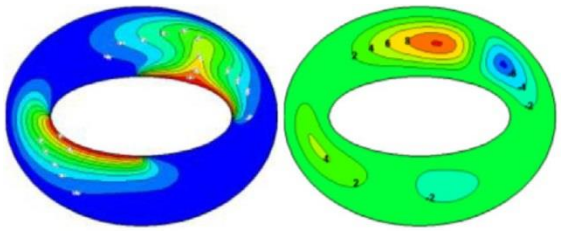

Ra=10^4 and ϕ=0.04

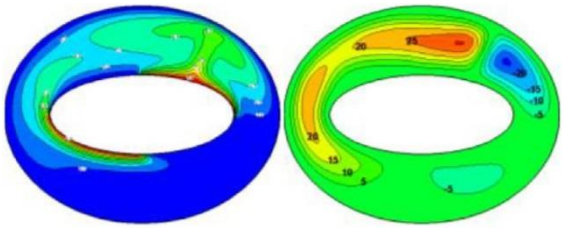

Ra=10^5 and ϕ=0.08

Figure 9. Isotherms (left) and streamlines (right) for different values of Rayleigh number Ra and volume fractions ϕ for Case 3.

Figure 10 highlights the changes of the average Nusselt number with different Rayleigh numbers for the inner and outer cylinder of model 3. It can be seen that increasing Rayleigh number and the nanoparticle volume fraction lead to higher heat transfer and the average Nusselt number. For instance, in compared Rayleigh of 10^3 with 10^5 in the constant nanoparticle volume fraction of 8%, the Nusselt number is increased by 4% on the inner and outer surfaces.

Finally, it should be declared that the utilization of nanofluids is recommended and Case 2 has the best thermal performance among all studied cases and is followed by Case 3 and Case 1.

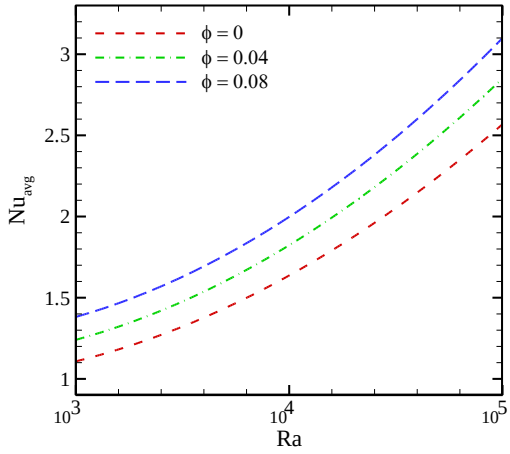

(a)

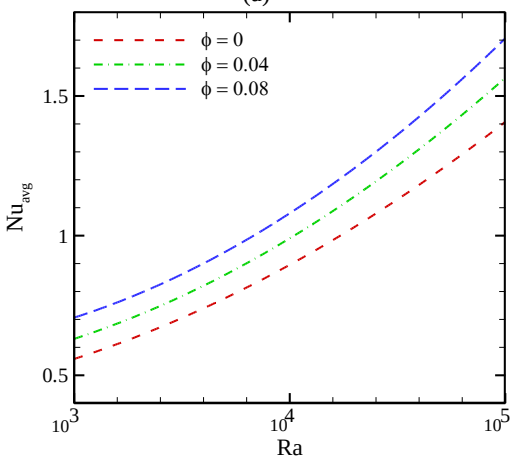

(b)

Figure 10. Effect of Rayleigh number Ra on average Nusselt number for different volume fractions ϕ (a) on the inner cylinder; (b) on the outer cylinder for Case 3

4. CONCLUSION

In this study, the effect of AlOOH – water nanofluids on the natural convection for 2 elliptical cylinders was numerically investigated. Three different models were simulated and compared under various temperature conditions, nanoparticles volume fractions ($0 < \phi < 0.08$) and Rayleigh numbers ($10^3 < Ra < 10^5$). The results can be summarized as follows:

- the higher Rayleigh number leads to more convection heat transfer
- At Ra $=10^5$, the Nusselt number and the stream function increased 130% and 20 times, respectively.
- The effect of Rayleigh number was much more dramatic than the volume fraction
- The Nusselt number of Case 2 was 25% and 60% higher than Case 3 and Case 2, respectively, which is the best model.

References

[1] J. A. Eastman, U. Choi, S. Li, L. Thompson, S. J. M. O. P. L. Lee, Enhanced thermal conductivity through the development of nanofluids, Vol. 457, pp. 3, 1996.

[2] O. Mahian, L. Kolsi, M. Amani, P. Estellé, G. Ahmadi, C. Kleinstreuer, J. S. Marshall, M. Siavashi, R. A. Taylor, H. J. P. r. Niazmand, Recent advances in modeling and simulation of nanofluid flows-Part I: Fundamentals and theory, Vol. 790, pp. 1-48, 2019.

[3] N. Kumar, A. J. O.-E. R. Srivastava, Enhancement in NBE emission and optical band gap by Al doping in nanocrystalline ZnO thin films, Vol. 26, No. 1, pp. 1-10, 2018.

[4] E. Ebrahimnia-Bajestan, M. Charjouei Moghadam, H. Niazmand, W. Daungthongsuk, S. Wongwises, Experimental and numerical investigation of nanofluids heat transfer characteristics for application in solar heat exchangers, *International Journal of Heat and Mass Transfer*, Vol. 92, pp. 1041-1052, 2016/01/01/, 2016.

[5] F. J. H. T. A. R. Mebarek-Oudina, Convective heat transfer of Titania nanofluids of different base fluids in cylindrical annulus with discrete heat source, Vol. 48, No. 1, pp. 135-147, 2019.

[6] T. Tayebi, A. J. J. N. H. T. Chamkha, Part A: Applications, Free convection enhancement in an annulus between horizontal confocal elliptical cylinders using hybrid nanofluids, Vol. 70, No. 10, pp. 1141-1156, 2016.

[7] M. Sheikholeslami, R. Ellahi, C. J. M. P. i. E. Fetecau, CuO–Water nanofluid magnetohydrodynamic natural convection inside a sinusoidal annulus in presence of melting heat transfer, Vol. 2017, 2017.

[8] M. Sheikholeslami, Z. Ziabakhsh, D. J. C. Ganji, S. A. Physicochemical, E. Aspects, Transport of Magnetohydrodynamic nanofluid in a porous media, Vol. 520, pp. 201-212, 2017.

[9] H. Dawood, H. Mohammed, K. J. C. S. i. T. E. Munisamy, Heat transfer augmentation using nanofluids in an elliptic annulus with constant heat flux boundary condition, Vol. 4, pp. 32-41, 2014.

[10] J. P. Dulhani, S. Sarkar, A. J. I. J. o. H. Dalal, M. Transfer, Effect of angle of incidence on mixed convective wake dynamics and heat transfer past a square cylinder in cross flow at Re= 100, Vol. 74, pp. 319-332, 2014.

[11] A. Dhiman, R. Chhabra, V. J. I. J. o. H. Eswaran, M. Transfer, Flow and heat transfer across a confined square cylinder in the steady flow regime: effect of Peclet number, Vol. 48, No. 21-22, pp. 4598-4614, 2005.

[12] V. Etminan-Farooji, E. Ebrahimnia-Bajestan, H. Niazmand, S. J. I. J. o. H. Wongwises, M. Transfer, Unconfined laminar nanofluid flow and heat transfer around a square cylinder, Vol. 55, No. 5-6, pp. 1475-1485, 2012.

[13] C.-C. Wang, C.-K. J. I. J. o. H. Chen, M. Transfer, Forced convection in a wavy-wall channel, Vol. 45, No. 12, pp. 2587-2595, 2002.

[14] J. Yin, G. Yang, Y. J. E. P. Li, The effects of wavy plate phase shift on flow and heat transfer characteristics in corrugated channel, Vol. 14, pp. 1566-1573, 2012.

[15] L. Zhang, D. J. N. H. T. Che, Part A: Applications, Turbulence models for fluid flow and heat transfer between cross-corrugated plates, Vol. 60, No. 5, pp. 410-440, 2011.

[16] S. Z. Heris, M. N. Esfahany, G. J. N. H. T. Etemad, Part A: Applications, Numerical investigation of nanofluid laminar convective heat transfer through a circular tube, Vol. 52, No. 11, pp. 1043-1058, 2007.

[17] S. Sadripour, A. J. J. T. S. Chamkha, E. Progress, The effect of nanoparticle morphology on heat transfer and entropy generation of supported nanofluids in a heat sink solar collector, Vol. 9, pp. 266-280, 2019.

[18] A. A. A. Arani, S. Sadripour, S. J. I. J. o. M. S. Kermani, Nanoparticle shape effects on thermal-hydraulic performance of boehmite alumina nanofluids in a sinusoidal–wavy mini-channel with phase shift and variable wavelength, Vol. 128, pp. 550-563, 2017.

[19] T. H. Kuehn, R. J. J. I. J. o. H. Goldstein, M. Transfer, Numerical solution to the Navier-Stokes equations for laminar natural convection about a horizontal isothermal circular cylinder, Vol. 23, No. 7, pp. 971-979, 1980.